Journal of Computational Acoustics, Vol. 20, No. 4 (2012) 1250009 (17 pages)

DOI: 10.1142/S0218396X12500099

INTERNATIONAL ASSOCIATION
FOR MATHEMATICS AND
COMPUTERS IN SIMULATION

ACOUSTIC WAVEFRONT TRACING IN INHOMOGENEOUS, MOVING MEDIA

NIKOLAY A. ZABOTIN

Department of Electrical,
Energy and Computer Engineering and Cooperative
Institute for Research in Environmental Sciences
University of Colorado at Boulder
Boulder, Colorado 80309, USA
Nikolay.Zabotin@Colorado.edu

OLEG A. GODIN

Cooperative Institute for Research in Environmental Sciences
University of Colorado at Boulder
and
NOAA/ESRL, Physical Sciences Division
Boulder, Colorado 80305, USA
Oleg.Godin@noaa.gov

PAUL C. SAVA

Center for Wave Phenomena
Colorado School of Mines
Golden, CO 80401, USA
psava@mines.edu

LIUDMILA Y. ZABOTINA

Department of Electrical,
Energy and Computer Engineering
University of Colorado at Boulder
Boulder, Colorado 80309, USA
Liudmila.Zabotina@Colorado.edu

Received 11 September 2011
Accepted 6 February 2012
Published 7 June 2012

We extend the Huygens wavefront tracing algorithm, which is a part of an open source Madagascar project, to sound propagation in inhomogeneous, moving media and apply it to a series of benchmark tasks. One set of tasks admits exact analytic solutions and serves the purpose of validation of the new algorithm. Another set of calculations demonstrates applicability of the algorithm to the studies of wavefront dynamics and stability in ocean and atmospheric acoustics. The method is based on a system of differential equations equivalent to the eikonal equation, but formulated in the ray

coordinate system. In this paper, we present a first-order, two-dimensional discretization scheme that is interpreted very simply in terms of the Huygens' principle. The method has proved to be a convenient alternative to conventional ray tracing.

Keywords: Wavefronts; timefronts; wavefronts tracing; moving media; irregular media; geometrical acoustics; underwater acoustics.

1. Introduction

In current mathematical[1–5] and geophysical[6–11] literature, a considerable attention is devoted to decreasing running time and improving accuracy of computer models of wave fields within the geometric optics (geometric acoustics) approximation through replacing traditional ray tracing approaches with more efficient numerical methods of solving the eikonal and transport equations. Solutions of the eikonal equation determine wave travel times and geometry of wavefronts, while corresponding solutions to the transport equation determine wave amplitude in the geometric optics (geometric acoustics) approximation.[12] Improvement of efficiency, stability, and accuracy of geometric optic (geometric acoustic) propagation models is particularly important in solving nonlinear inverse problems,[13–16] Monte-Carlo simulations of wave propagation through random media,[17–20] and in investigations of interferometry of imperfectly diffuse noise fields.[21–24]

A major problem with a direct modeling of acoustic wavefronts in the complex media like ocean or atmosphere without solving ray tracing equations (for example, through numerical solution of the eikonal equation) lies in the eikonal (and acoustic travel time) being a multi-valued function of position. A number of computational approaches to solve the eikonal equation without ray tracing have been developed in mathematical and seismological communities.[1,7,25,26] Most of these methods are only capable of tracing the wavefront of the earliest, first arrival and thus are not suitable for acoustic applications in complex multi-scale media. In addition they all lack ability to deal with moving media.

The new algorithm presented in this paper is an adaptation and extension of the computer codes originally developed by Sava and Fomel[6,27] for seismic modeling and imaging. These codes implement an approach known as Huygens wavefront tracing (HWT). HWT consists in solving by a finite-difference technique of a certain system of partial differential equations, which is equivalent to the eikonal equation but is formulated in the ray coordinate system. This should be contrasted with wavefront construction using traditional ray tracing, where the eikonal equation is solved by numerically integrating a large number of ordinary differential equations describing individual rays. For wavefront tracing in inhomogeneous media, HWT is much more computationally efficient and robust than traditional ray codes.[6] Unlike many other eikonal solvers, the HWT method produces the output in ray coordinates and has the important ability to track multiple arrivals. With the HWT method, each wavefront is generated from the preceding one by finite differences in the ray-coordinates domain. The first-order discretization scheme for HWT has a remarkably simple interpretation in terms of the Huygens principle, hence the method's name. Basic algorithm implementing HWT is a part of an open source Madagascar project (http://www.reproducibility.org). The

choice of HWT as the basis of acoustic wavefront modeling was also motivated by the fact that the Huygens principle remains valid in moving media[28] and, therefore, it should be possible to describe within the HWT framework the acoustic effects due to currents in the ocean and winds in the atmosphere.

As a part of adaptation of the HWT technique it has proved necessary to modify the underlying finite-difference algorithm to improve stability of wavefront predictions at long-range propagation in media with a wide range of spatial scales of inhomogeneities. Based on theoretical results on properties of acoustic rays and wavefronts in inhomogeneous anisotropic environments,[29,30] the HWT technique has been extended to moving fluids. Functionality has been developed to efficiently model acoustic timefronts[17] in addition to the wavefronts.

Verification of the new numerical model of wavefront propagation required formulation of several benchmark problems. The algorithm reproduces acoustic wavefronts caused by a static point source in a homogeneous fluid uniformly moving with a sub-sonic speed. New explicit, analytic solutions of the eikonal equation for wavefronts due to a point source in fluids with a uniform flow and linear profiles of either the sound speed or the refractive index squared, as well as for a fluid with linear profiles of the sound speed and the flow velocity, have been utilized for validation purposes.

Application of wavefront tracing to simulation of long-range sound propagation in the ocean with a random internal gravity wave field described by the Garrett–Munk spectrum has been demonstrated. The high-resolution, multi-mode model of the internal gravity wave field employed in our simulations is described in Ref. 29. At the present stage, the internal wave model predicts only random sound-speed perturbations but not the random currents caused by the internal waves. For the purposes of the current publication three-dimensional effects are not yet accounted for in the sound propagation model.

2. Basic Theory

We shall consider acoustic rays and wavefronts in a two-dimensional fluid with sound speed $c(\mathbf{x})$ and flow velocity $\mathbf{u}(\mathbf{x}) = \{u_x(\mathbf{x}), u_z(\mathbf{x})\}$. Fluid parameters are assumed to be smooth functions of position $\mathbf{x} = \{x, z\}$. (In geophysical applications, x and z have meanings of horizontal and vertical coordinates, respectively.) Let a ray $\mathbf{x} = \mathbf{r}(t, \gamma)$ be parameterized as a function of time t and a parameter γ that specifies the ray, such as the angle that determines direction of the ray launch from a point source or the position of the launch point on an initial wavefront. The set $\{t, \gamma\}$ can be viewed as ray coordinates. Let $\mathbf{s}$ stand for the slowness vector at a point on the ray. (The ray trajectory and wavefront geometry as well as group velocity and slowness are independent of wave frequency. For waves of frequency ω, wave vector $\mathbf{k} = \omega\mathbf{s}$.)

Eikonal equation[12] in moving media is

$$\mathbf{s} \cdot \mathbf{u} + sc = 1, \quad \mathbf{s} = \nabla\Psi, \tag{1}$$

where Ψ is the eikonal. By definition, the eikonal (and consequently, the travel time) is constant on the wavefronts. Differential equations of rays can be written as[30,31]

$$\frac{d\mathbf{r}}{dt} = \mathbf{u} + c\frac{\mathbf{s}}{s}, \tag{2}$$

$$\frac{ds_\alpha}{dt} = -s\frac{\partial c}{\partial x_\alpha} - s_\beta \frac{\partial u_\beta}{\partial x_\alpha}. \tag{3}$$

Here $\alpha, \beta = 1, 2$ and summation over repeated indices is implied in this section (but not in the next section). Ray equations (2) and (3) are ordinary differential equations; d/dt are actually partial time derivatives taken with γ kept constant. Group velocity of sound is

$$\mathbf{c}_g = \mathbf{u} + cs^{-1}\mathbf{s}. \tag{4}$$

For derivatives $\mathbf{R} = \partial\mathbf{r}/\partial\gamma$ of the ray trajectory with respect to the initial conditions, it is shown in Ref. 30 that the inner product

$$\mathbf{s} \cdot \mathbf{R} = 0 \tag{5}$$

at every point on a ray, if the product is zero at any one point on the ray. We will assume that γ is chosen to satisfy the latter condition. For rays emanating from a point source, Eq. (5) holds for any parameterization of the rays provided the fluid is homogeneous in a small vicinity of the source. (Equation (5) always holds in the motionless case.[30])
From Eq. (2), we have

$$\left(\frac{d\mathbf{r}}{dt} - \mathbf{u}\right)^2 = c^2. \tag{6}$$

From Eqs. (2) and (5) it follows that

$$\left(\frac{d\mathbf{r}}{dt} - \mathbf{u}\right) \cdot \frac{\partial\mathbf{r}}{\partial\gamma} = 0. \tag{7}$$

Let us add here a convenient relation between directions of the wave normal and the acoustic ray in moving fluids. The direction of a ray at a given point is given by the unit vector $\mathbf{m} = \mathbf{c}_g/c_g$ tangent to the ray and the unit normal to the wavefront at the same point is $\mathbf{n} = \mathbf{s}/s$. $\mathbf{n}$ points in the direction of the wavefront propagation (expansion), while $\mathbf{m}$ points in the direction of sound energy propagation along the ray. When $\mathbf{n}$ is known, as it follows from (4),

$$\mathbf{m} = \frac{\mathbf{n} + \mathbf{u}/c}{\sqrt{1 + \dfrac{u^2}{c^2} + 2\mathbf{n} \cdot \dfrac{\mathbf{u}}{c}}}. \tag{8}$$

The inverse relation takes the form[31]

$$\mathbf{n} = \mathbf{m}\sqrt{1 - \frac{u^2}{c^2} + \left(\mathbf{m} \cdot \frac{\mathbf{u}}{c}\right)^2} - \frac{\mathbf{u}}{c} + \mathbf{m}\left(\mathbf{m} \cdot \frac{\mathbf{u}}{c}\right). \tag{9}$$

Here, as before, $\mathbf{u}$ and c are the flow velocity and the sound speed.

3. Discretization Scheme

Consider a shift of a wavefront over a small time interval δt. Let $a = c\delta t$. The quantity a corresponds to r in Ref. 27. Let $\mathbf{r} = (x(t,\gamma), z(t,\gamma))$, where (x, z) are Cartesian coordinates, and

$$\mathbf{u}/c = (\mu_x, \mu_z). \tag{10}$$

By adopting the notation for discrete mesh in (t,γ) where index i enumerates rays and index j enumerates time steps, from (6) we obtain the following finite difference equation:

$$(x^i_{j+1} - x^i_j - \mu^i_{x;j}a^i_j)^2 + (z^i_{j+1} - z^i_j - \mu^i_{z;j}a^i_j)^2 = (a^i_j)^2. \tag{11}$$

If (x, z) is a point on a new wavefront reached at time $t + \delta t$, then, according to Eq. (6),

$$(x - x(t,\gamma) - \mu_x(t,\gamma)a(t,\gamma))^2 + (z - z(t,\gamma) - \mu_z(t,\gamma)a(t,\gamma))^2 = a^2(t,\gamma). \tag{12}$$

By differentiating Eq. (12) with respect to γ and approximating derivatives by finite differences, we obtain

$$\begin{aligned}(x^i_j - x^i_{j+1} + \mu^i_{x;j}a^i_j)[x^{i+1}_j - x^{i-1}_j + a^i_j(\mu^{i+1}_{x;j} - \mu^{i-1}_{x;j}) + \mu^i_{x;j}(a^{i+1}_j - a^{i-1}_j)]\\ + (z^i_j - z^i_{j+1} + \mu^i_{z;j}a^i_j)[z^{i+1}_j - z^{i-1}_j + a^i_j(\mu^{i+1}_{z;j} - \mu^{i-1}_{z;j}) + \mu^i_{z;j}(a^{i+1}_j - a^{i-1}_j)]\\ = a^i_j(a^{i+1}_j - a^{i-1}_j).\end{aligned} \tag{13}$$

Our Eqs. (6), (7), (11) and (13) are moving-medium counterparts, respectively, of Eqs. (5)–(7) and (10) in Ref. 27 and reduce to the latter when $\mathbf{u} \to 0$.

The explicit scheme based on Eqs. (11) and (13) determines the next, $(j+1)$th position of the wavefront on a base ray path i from coordinates of three points on a previous wavefront j. As in the case of a motionless fluid, the set of Eqs. (11) and (13) is a direct expression of the Huygens' principle.

An analysis shows that solution of the difference equations (11) and (13) converges to the solution of the differential equations (6) and (7), with the discrepancy decreasing linearly with the step size of the difference scheme.

4. Implementation Details

4.1. *Initialization*

The system of Eqs. (11) and (13) requires prior knowledge of the shape of the initial wavefront. In the case of a point source, one can assume that both the sound speed $c(\mathbf{x})$ and the flow velocity $\mathbf{u}(\mathbf{x})$ vary smoothly in the vicinity of the source point $\{x_0, z_0\}$ and that their spatial variation within the very first step of the scheme can be neglected. Then coordinates

of base points on the first wavefront may be obtained from Eq. (4):

$$\begin{aligned} x_1^i &= x_0 + c(x_0, z_0) \cdot \delta t \cdot \sin(\vartheta_i) + u_x(x_0, z_0) \cdot \delta t; \\ z_1^i &= z_0 + c(x_0, z_0) \cdot \delta t \cdot \cos(\vartheta_i) + u_z(x_0, z_0) \cdot \delta t, \end{aligned} \tag{14}$$

where base ray paths are characterized by the angle of the ray launch ϑ_i counted counterclockwise from the direction of the z-axis.

4.2. *One step of the scheme*

The systems (11), (13) reduces to a quadratic equation and has the following two explicit solutions:

$$\begin{aligned} x_{j+1}^i &= x_j^i + \mu_{x;j}^i a_j^i - a_j^i (A_j^i G_j^i \pm B_j^i H_j^i); \\ z_{j+1}^i &= z_j^i + \mu_{z;j}^i a_j^i - a_j^i (A_j^i H_j^i \mp B_j^i G_j^i), \end{aligned} \tag{15}$$

where

$$\begin{aligned} A_j^i &= F_j^i [(H_j^i)^2 + (G_j^i)^2]^{-1}, \\ B_j^i &= \operatorname{sgn}(G_j^i) [(H_j^i)^2 + (G_j^i)^2 - (F_j^i)^2]^{0.5} [(H_j^i)^2 + (G_j^i)^2]^{-1}, \\ F_j^i &= a_j^{i+1} - a_j^{i-1}, \\ G_j^i &= x_j^{i+1} - x_j^{i-1} + a_j^i (\mu_{x;j}^{i+1} - \mu_{x;j}^{i-1}) + \mu_{x;j}^i F_j^i, \\ H_j^i &= z_j^{i+1} - z_j^{i-1} + a_j^i (\mu_{z;j}^{i+1} - \mu_{z;j}^{i-1}) + \mu_{z;j}^i F_j^i, \end{aligned}$$

and no summation over repeated indices is implied. Only one of the two points described by (15) makes physical sense. The correct solution is the one represented by the point farthest away from the preceding one on the same ray. In the case of moving fluid, this condition should be supplemented by explicit check of the absence of an unphysical sharp turn of the ray. Reflections from boundaries are treated in the special way described in Sec. 4.3.

Note that, though indices $i+1, i-1$ in expression (15) denote the rays adjacent to the base ray i, there is no requirement that these rays would necessarily belong to the base ray set defined on the original wavefront. To calculate the next, $(j+1)$th wavefront position on the base ray path i, one can introduce two auxiliary rays crossing the jth wavefront that are characterized by small, equal in absolute value but opposite in sign, shifts in any parameter that distinguishes them from the ray i. For example, this parameter may describe positions of the two rays on the wavefront j relative to the ray i. In a small vicinity of the point (x_j^i, z_j^i) the wavefront j may be approximated by a segment of a straight line orthogonal to the unit vector $\mathbf{n}$ described by expression (9). The two points on this line that are shifted in opposite directions with relation to the point (x_j^i, z_j^i) by the same small distances a_j^i can be used to substitute x_j^{i-1}, z_j^{i-1} and x_j^{i+1}, z_j^{i+1} in Eq. (15). This approach using auxiliary neighbor rays instead of the base adjacent rays provides stability to the scheme even under

the conditions of very long propagation paths in irregular media (such as ocean), where spatial distribution of the base ray crossings with wavefronts becomes highly uneven. The simple approximation of a plane wavefront segment in a small vicinity of the point (x_j^i, z_j^i) can, of course, be replaced with a more elaborate approximation by taking into account available information about positions of the other points on the wavefront.

4.3. *Reflection at a boundary*

In stationary media (meaning that $c(\mathbf{x})$ and $\mathbf{u}(\mathbf{x})$ do not depend on time and boundaries are motionless in the absence of sound) normal component of the flow velocity vanishes on the boundary.[12] Let a boundary be locally described by a unit tangent vector $\mathbf{b}(\mathbf{x})$. Then, in the 2-D problem $\mathbf{u} \parallel \mathbf{b}$ at the points belonging to the boundary, and the reflection condition[12] for a wavevector reduces to conservations of its absolute value and of its projection onto the $\mathbf{b}$ vector direction. As immediately follows from (4), the absolute value of the $\mathbf{c}_g$ vector and its projection onto the $\mathbf{b}$ vector direction are also preserved. This means that a simple specular reflection condition (the angle of incidence equals the angle of reflection) is valid for the ray path itself. For rectilinear boundaries of the kind

$$z = bx + d, \tag{16}$$

where b and d are constants, processing of the reflection cases starts with a check at every step of the scheme if the new position of the wavefront $\mathbf{x}_{j+1}^i$ and the previous position of the wavefront $\mathbf{x}_j^i$ appear at different sides of the line (16). If the result of the check is positive, then the point $\mathbf{x}_{j+1}^i$ is replaced with the point $\tilde{\mathbf{x}}_{j+1}^i$ symmetrical to the point $\mathbf{x}_{j+1}^i$ with respect to the line (16). This is the next position of the wavefront on the base ray i. For the next step of calculations (described in Sec. 4.2) the previous position of the wavefront $\mathbf{x}_j^i$ is replaced with an auxiliary point $\tilde{\mathbf{x}}_{j+1}^i$ symmetrical to the point $\mathbf{x}_j^i$ with respect to the line (16).

5. Examples of Calculations

The following examples serve for verification purposes and demonstrate capabilities of the new version of the software. We start with two simple examples of motionless fluid to confirm that the new algorithm accurately reproduces old capabilities. Then we include currents into the medium models and compare specially obtained analytical solutions to numerical calculations. Finally we show how new algorithm reproduces basic properties of the rays and the time fronts for a long range propagation of the sound in irregular ocean.

5.1. *Motionless fluid with linear sound speed profile*

Consider fluid half-space $z > 0$ with linear dependence of the sound speed on the depth:

$$c(z) = \alpha z, \quad \alpha = \text{const.} > 0. \tag{17}$$

Let a point sound source be located at the point (0, 0, z_0) in 3-D space. An exact analytic solution for acoustic field due to a point monochromatic source in such a medium was

obtained by Pekeris[32] and is given by Eq. (4.3.38) in Ref. 12. By calculating high-frequency asymptotics of the phase of the exact solution of the wave equation, for the ray travel time to point (x, y, z) we obtain

$$t = \frac{2}{\alpha}\operatorname{arctanh}\sqrt{\frac{x^2 + y^2 + (z - z_0)^2}{x^2 + y^2 + (z + z_0)^2}}. \tag{18}$$

It is straightforward to check that $t(x, y, z)$ (18) satisfies eikonal Eq. (1), which in motionless fluid becomes $c^2(\nabla t)^2 = 1$, and tends to zero when receiver approaches the point source. For receivers in the plane $y = 0$, the travel time from the point source coincides with the travel time from a linear source at $(0, y_0, z_0)$ and, hence, the travel time in 2-D propagation problem.

In the plane $y = 0$, Eq. (18) can be rearranged as an explicit equation for wavefronts:

$$x^2 + (z - z_0 \cosh \alpha t)^2 = z_0^2 \sinh^2 \alpha t. \tag{19}$$

This is an equation of a circle with a radius that increases with time. The center of the circle, which at $t = 0$ coincides with the source, also shifts with time. Times fronts are given by the explicit equation

$$z = z_0 \cosh \alpha t \pm \sqrt{z_0^2 \sinh^2 \alpha t - x^2}. \tag{20}$$

Figures 1(a) and 1(b) compare results of numerical wavefront/timefront tracing using new generalized code to analytical results described by Eqs. (19) and (20).

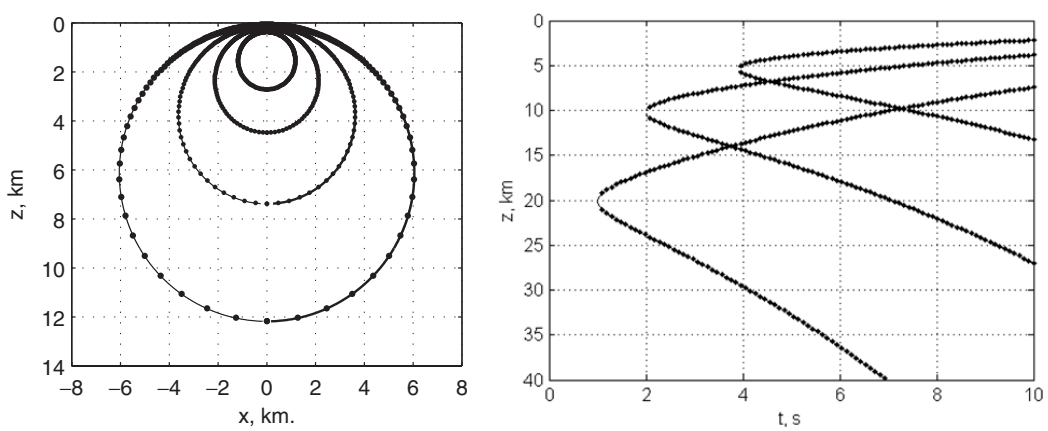

(a) (b)

Fig. 1. (a) Wavefronts calculated by HWT algorithm (circles) for the model of sound speed $c(z) = \alpha z$ (where $\alpha = 0.1\,\mathrm{km}^{-1}$) and the model of current velocity $\mathbf{u} = 0$, with a source located at $x = 0$, $z = 1\,\mathrm{km}$, compared to analytical solution (20) (lines) for the sequence of times $t = 10\,\mathrm{s}$, $15\,\mathrm{s}$, $20\,\mathrm{s}$, $25\,\mathrm{s}$. (b) Timefronts calculated by the extended HWT algorithm (circles) for the same environmental model, compared to analytical solution (20) (lines) for $x = 2\,\mathrm{km}$ and for the three source locations on the line $x = 0$: (1) $z = 5$, (2) $z = 10$ and (3) $z = 20\,\mathrm{km}$.

5.2. *Motionless fluid with linear profile of the refraction index squared*

As another example, consider fluid with the sound speed profile

$$c(z) = c_0/\sqrt{1 - 2bz}. \tag{21}$$

Here, c_0 has a meaning of sound speed at $z = 0$ and b is a constant coefficient. The fluid occupies the half-space, where $2bz < 1$. Again, let a point sound source be located at the point (0, 0, z_0) in 3-D space. An exact analytic solution for acoustic field due to a point monochromatic source in such a medium was obtained by Li *et al.*[33] and is given by Eq. (4.3.54) in Ref. 12. By calculating high-frequency asymptotics of the exact solution of the wave equation, for the ray travel times to point (x, y, z) we obtain two results:

$$t = \frac{1}{3c_0|b|}\{[1 + |b|\sqrt{x^2 + y^2 + (z - z_0)^2} - b(z + z_0)]^{3/2} \pm [1 - |b|\sqrt{x^2 + y^2 + (z - z_0)^2} - b(z + z_0)]^{3/2}\}. \tag{22}$$

The minus and plus signs in Eq. (22) correspond, respectively, to wavefronts of "direct" and "refracted" waves. All rays corresponding to the refracted wave have turning points, where their group velocity is orthogonal to the sound speed gradient, before reaching the receiver at the point (x, y, z). Rays corresponding to the direct wave have no turning points. An inspection shows that both travel times $t(x, z)$ (22) satisfy eikonal Eq. (1), as expected. Travel time of the direct wave (22), but not of the refracted wave, tends to zero when receiver approaches the point source.

For receivers in the plane $y = 0$, the travel time from the point source in the 3-D problem coincides with the travel time in the 2-D problem we solve numerically. Figure 2 demonstrates how well the new numerical scheme reproduces time fronts described by Eq. (22).

Using Eqs. (19) and (22), benchmark problems can be also constructed for wavefronts and timefronts in a moving fluid with a uniform horizontal current and sound speeds (17) or (21). If current velocity $\mathbf{u} = (u_0, 0)$ and $u_0 = \text{const.}$, Eqs. (18)–(20) and Eq. (22) remain valid in the moving fluid, with a substitution

$$x^2 \to (x - u_0 t)^2. \tag{23}$$

Figures 3(a) and 3(b) show results of numerical calculations of the timefronts for the two models of the propagation medium with a homogeneous current, compared to the analytical solutions.

5.3. *Moving fluid with linear sound speed and flow velocity profiles*

Consider acoustic rays and wavefronts in a 2-D layered fluid with sound speed (17) and background flow velocity

$$\mathbf{u} = \{u_0(1 + \gamma z), 0\}, \tag{24}$$

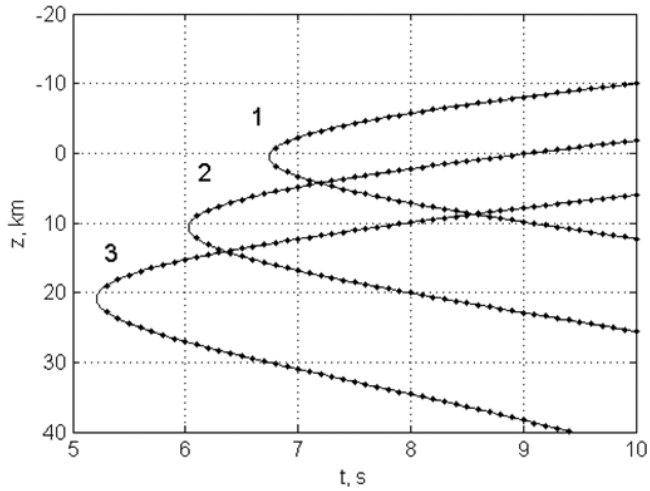

Fig. 2. Timefronts calculated by the extended HWT algorithm (circles) for the model of sound speed $c(z) = c_0/\sqrt{1-2bz}$ (where $c_0 = 1.48\,\mathrm{km/s}$, $b = 0.01\,\mathrm{km}^{-1}$) and the model of current velocity $\mathbf{u} = 0$, compared to analytical solution (22) (lines) for $x = 10\,\mathrm{km}$ and for the three source locations on the line $x = 0$: (1) $z = 0$, (2) $z = 10$ and (3) $z = 20\,\mathrm{km}$.

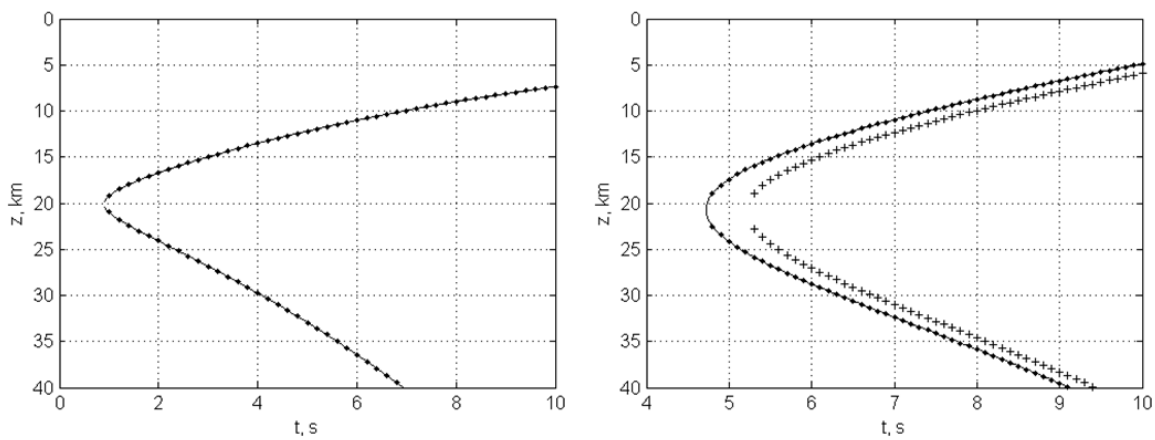

(a) (b)

Fig. 3. (a) Timefront calculated by HWT algorithm (circles) for the model of sound speed $c(z) = \alpha z$ (where $\alpha = 0.1\,\mathrm{km}^{-1}$) and the model of current velocity $\mathbf{u} = (u_0, 0)$, $u_0 = 0.2\,\mathrm{km/s}$, for $x = 2\,\mathrm{km}$, with a source located at $x = 0$, $z = 20\,\mathrm{km}$, compared to analytical solutions (20) and (23) (line). (b) Timefront calculated by HWT algorithm (circles) for the model of sound speed $c(z) = c_0/\sqrt{1-2bz}$ (where $c_0 = 1.48\,\mathrm{km/s}$, $b = 0.01\,\mathrm{km}^{-1}$) and the model of current velocity $\mathbf{u} = (u_0, 0)$, $u_0 = 0.2\,\mathrm{km/s}$, for $x = 10\,\mathrm{km}$, with a source located at $x = 0$, $z = 20\,\mathrm{km}$, compared to analytical solutions (22) and (23) (line). Also shown is the time front for the same conditions but $u_0 = 0$ (crosses).

where γ is a constant. Unlike the simpler models considered above, this environmental model allows us to benchmark the new wavefront tracing algorithm in a medium where both sound speed and flow velocity are inhomogeneous.

In any layered medium, where $u_z = 0$ and c and u_x are functions of coordinate z only, the component s_x of the slowness vector remains constant on each ray, according to Eq. (3), and $s = (1 - s_x u_x)/c$, according to Eq. (1). Then, the differential Eqs. (2) and (3) of rays can be written as

$$\frac{dx}{dz} = \frac{u_x(1 - s_x u_x) + s_x c^2}{c\sqrt{(1 - s_x u_x)^2 - s_x^2 c^2}}, \quad \frac{dt}{dz} = \frac{1 - s_x u_x}{c\sqrt{(1 - s_x u_x)^2 - s_x^2 c^2}}, \tag{25}$$

which are readily integrated in quadratures for x and t as functions of s_x (or launch angle of the ray) and z.[12] In a fluid with linear profiles (17) and (24) of the sound speed and flow velocity, the resulting integrals can be evaluated in a closed form.
We assume for definiteness that

$$\alpha \geq |\gamma u_0|, \quad \alpha z_0 > |u_0(1 + \gamma z_0)|. \tag{26}$$

Let a point sound source be located at the point $(0, z_0)$, $z_0 > 0$. Consider a ray, for which the wave normal $\mathbf{n}$ makes a grazing angle χ with Ox coordinate axis at the source. Then $\mathbf{n} = (\cos\chi, \sin\chi)$ at $z = z_0$, where $-\pi < \chi \leq \pi$. Under conditions (26), rays with $-\pi < \chi < 0$ have no turning points, and rays with $0 \leq \chi \leq \pi$ have at most one turning point. For rays without turning points, $z > z_0$ when $\chi > 0$ and $z < z_0$ when $\chi < 0$. For such rays, their geometry and acoustic travel time from the source are given by the following algebraic equations:

$$\begin{aligned} x(z,\chi) = \Bigg[& \frac{u_0 z_0(\alpha + \gamma u_0 \cos\chi)}{\alpha^2\sqrt{1 - \gamma^2 u_0^2/\alpha^2}|\cos\chi|} f_1(a,b,z) + \frac{\gamma u_0}{\alpha^2\sqrt{1 - \gamma^2 u_0^2/\alpha^2}} \\ & \times \left(\frac{\alpha z_0}{|\cos\chi|} - u_0(1 - \gamma z_0)\,\mathrm{sgn}\,(\cos\chi) \right) f_2(a,b,z) \\ & + \ \mathrm{sgn}\,(\cos\chi)\sqrt{1 - \frac{\gamma^2 u_0^2}{\alpha^2}} f_3(a,b,z) \Bigg] \Bigg|_{z=z_-}^{z=z_+}, \end{aligned} \tag{27}$$

$$t(z,\chi) = \left[\frac{\gamma u_0\,\mathrm{sgn}\,(\cos\chi) + \alpha/|\cos\chi|}{\alpha^2\sqrt{1 - \gamma^2 u_0^2/\alpha^2}} z_0 f_1(a,b,z) - \frac{\gamma u_0\,\mathrm{sgn}\,(\cos\chi)}{\alpha^2\sqrt{1 - \gamma^2 u_0^2/\alpha^2}} f_2(a,b,z) \right] \Bigg|_{z=z_-}^{z=z_+}, \tag{28}$$

where $z_+ = \max(z, z_0)$, $z_- = \min(z, z_0)$,

$$a = z_0 \frac{\alpha + \gamma u_0 \cos\chi}{(\alpha - \gamma u_0\,\mathrm{sgn}\,(\cos\chi))|\cos\chi|}, \quad b = z_0 \frac{\alpha + \gamma u_0 \cos\chi}{(\alpha + \gamma u_0\,\mathrm{sgn}\,(\cos\chi))|\cos\chi|}, \tag{29}$$

$$f_1(a,b,z) = \frac{-1}{\sqrt{ab}} \ln \frac{2ab + (b-a)z + 2\sqrt{ab}\sqrt{(a+z)(b-z)}}{z}, \tag{30}$$

$$f_2(a,b,z) = -2\arctan\sqrt{\frac{b-z}{a+z}}, \tag{31}$$

$$f_3(a,b,z) = -\sqrt{(a+z)(b-z)} - \frac{a-b}{2}\arctan\frac{a-b+2z}{2\sqrt{(a+z)(b-z)}}. \tag{32}$$

Equations (27) and (28) can be viewed as a parametric description of wavefronts in the xz plane and an implicit description of the corresponding time fronts. For time fronts on a line $z = \text{const.}$, Eq. (28) provides an explicit parametric description so one can easily use this feature for comparisons with numerical solutions.

For rays with $\chi > 0$ that have a turning point (it is located at $z = b$), instead of Eqs. (27) and (28), we have

$$\begin{aligned} x(z,\chi) = {} & \frac{-u_0 z_0(\alpha+\gamma u_0\cos\chi)}{\alpha^2\sqrt{1-\gamma^2u_0^2/\alpha^2}|\cos\chi|}\left[\frac{2\ln(a+b)}{\sqrt{ab}} + f_1(a,b,z) + f_1(a,b,z_0)\right] \\ & - \frac{\gamma u_0}{\alpha^2\sqrt{1-\gamma^2u_0^2/\alpha^2}}\left(\frac{\alpha z_0}{|\cos\chi|} - u_0(1-\gamma z_0)\operatorname{sgn}(\cos\chi)\right)[f_2(a,b,z) + f_2(a,b,z_0)] \\ & - \operatorname{sgn}(\cos\chi)\sqrt{1-\gamma^2u_0^2/\alpha^2}\left[\frac{\pi}{2}(a-b) + f_3(a,b,z) + f_3(a,b,z_0)\right], \end{aligned} \tag{33}$$

$$\begin{aligned} t(z,\chi) = {} & -\frac{\gamma u_0\operatorname{sgn}(\cos\chi) + \alpha/|\cos\chi|}{\alpha^2\sqrt{1-\gamma^2u_0^2/\alpha^2}} z_0\left[2\frac{\ln(a+b)}{\sqrt{ab}} + f_1(a,b,z) + f_1(a,b,z_0)\right] \\ & + \frac{\gamma u_0\operatorname{sgn}(\cos\chi)}{\alpha^2\sqrt{1-\gamma^2u_0^2/\alpha^2}}[f_2(a,b,z) + f_2(a,b,z_0)]. \end{aligned} \tag{34}$$

Equations (27)–(29), (33) and (34) are not applicable when $\cos\chi = 0$. On rays with $\chi = \pm\pi/2$, there are no turning points, the unit wave normal $\mathbf{n}$ is vertical, and

$$x\left(z,\chi = \pm\frac{\pi}{2}\right) = \frac{u_0}{\alpha}\left[\left|\ln\frac{z}{z_0}\right| + \gamma|z-z_0|\right], \quad t\left(z,\chi = \pm\frac{\pi}{2}\right) = \frac{1}{\alpha}\left|\ln\frac{z}{z_0}\right|. \tag{35}$$

Figure 4 provides a comparison between analytically and numerically determined time fronts for this model for three different positions of the $z = \text{const.}$ line. A point source was set at $x_0 = 0$, $z_0 = 10\,\text{km}$ and the following set of parameters described the propagation medium model: $\alpha = 0.1$, $\gamma = 0.15$ and $u_0 = 0.2\,\text{km/s}$. Exaggerated values of flow velocities have been utilized to illustrate accuracy of numerical predictions under more stringent conditions. In this and in other calculations, a convergence of the numerical solution to the analytical one has been tested and it has been confirmed that the differences between the two at any propagation ranges decrease linearly with the time step.

5.4. *Long-range sound propagation in the ocean*

As an example demonstrating the new algorithm performance in describing long-range propagation and reflections at linear boundaries let us consider at first a model of the ocean's

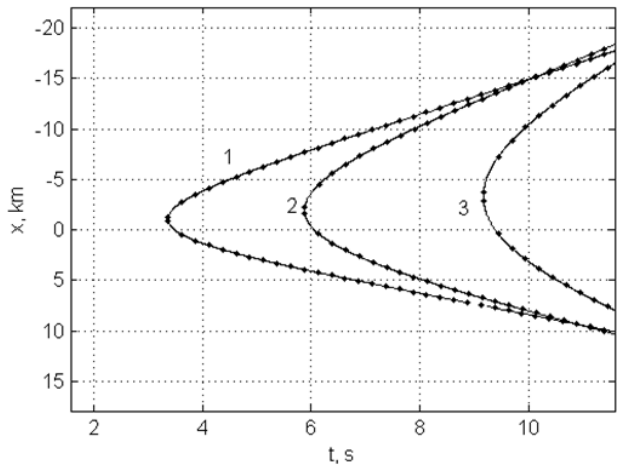

Fig. 4. Timefronts calculated by the extended HWT algorithm (circles) for the model of sound speed $c(z) = c_0/\sqrt{1-2bz}$ (where $c_0 = 1.48\,\mathrm{km/s}$, $b = 0.01\,\mathrm{km}^{-1}$) and the model of current velocity $\mathbf{u} = \{u_0(1+\gamma z), 0\}$ (where $u_0 = 0.2\,\mathrm{km/s}$ and $\gamma = 0.15\,\mathrm{km}^{-1}$) compared to analytical solutions (27)–(34) (lines) for the point source position $x_0 = 0$, $z_0 = 10\,\mathrm{km}$ and for three different positions of the $z = \mathrm{const.}$ line: (1) 14 km, (2) 18 km and (3) 25 km.

acoustical waveguide with the canonical sound speed profile (Ref. 34, p. 37)

$$c = c_0[1 + \chi(e^{2\zeta} - 2\zeta - 1)], \quad \zeta = (z - z_a)/H, \tag{36}$$

where $z_a = H = 1\,\mathrm{km}$, $c_0 = 1500\,\mathrm{m/s}$, and $\chi = 6.215 \cdot 10^{-3}$. The upper boundary is a horizontal line $z = 0$; the lower boundary is described by the equation $z = 5.0 + 0.01x$ where both x and z are expressed in km. The HWT algorithm focuses on wavefront propagation, but all information about the base ray paths set is also preserved. Figure 5 builds on this feature showing ray geometry in the 0–370 km range in the case of a point source located at $x_0 = 0$, $z_0 = 1\,\mathrm{km}$. Note the difference in the horizontal and vertical scales in the figure. Various types of rays [refracted rays trapped in the SOFAR channel, surface-reflected/bottom-reflected (SRBR) rays, surface-reflected/refracted rays (SRR)] as well as a transition from SRBR to SRR rays at downslope propagation are correctly reproduced by the extended HWT code, where rays are obtained as a byproduct of wavefront tracing.

Now we proceed with still more complex situation. In Fig. 6 timefronts in range-independent ocean are compared to timefronts in a single realization of an ocean with a random internal gravity wave field described by the Garrett–Munk spectrum. The high-resolution, multi-mode model of the internal gravity wave field employed in our simulation is described in Ref. 17 and was provided by Wolfson. The internal wave model[17] predicts random sound-speed perturbations but not the random currents caused by the internal waves. This simplification is actually not a requirement of the HWT numerical algorithm. Note also that multiple arrivals readily reproduced by the HWT algorithm are a very essential feature of the propagation picture in the ocean acoustic waveguide perturbed by internal waves.[17,35,36]

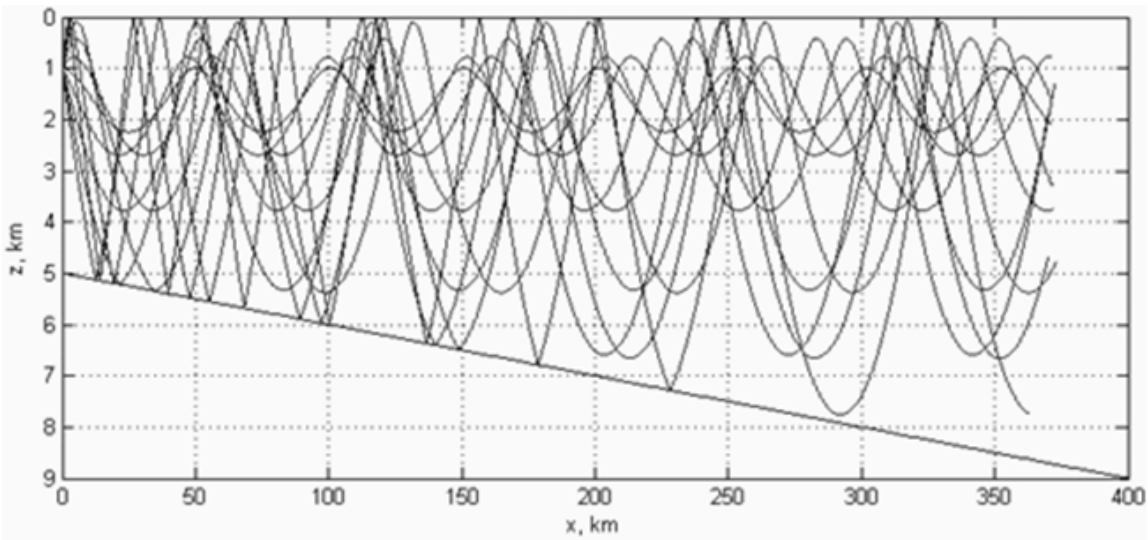

Fig. 5. Ray geometry in the problem of long-range sound propagation in the ocean waveguide with canonical sound speed profile described by Eq. (36) and with two reflecting boundaries ($z = 0$ and $z = 5.0 + 0.01x$, where both x and z are expressed in km), obtained with the extended HWT algorithm.

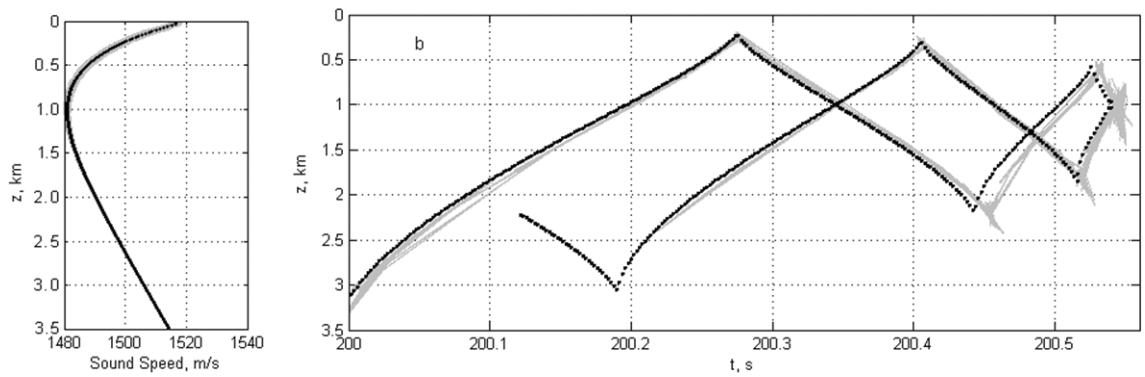

(a) (b)

Fig. 6. (a) Sound speed profiles for a model of the ocean waveguide with internal gravity waves at different ranges and range-averaged sound speed profile are shown in grey and black, respectively. (b) Acoustic time-fronts calculated with the extended HWT algorithm for a vertical line array at the range 297 km in an ocean with internal gravity waves (grey) are compared to the time fronts calculated for a range-independent ocean (black). A point source is located at $x = 0$, $z = 1$ km.

6. Conclusion

We have described a generalization of the HWT algorithm, a part of the open-source project Madagascar, to include sound propagation in inhomogeneous, moving fluids and reflections at sloping boundaries. Functionality has been developed to efficiently model acoustic time-fronts in addition to the wavefronts. To verify the new numerical algorithm of wavefront

tracing, several benchmark problems were formulated, including propagation of sound waves from a point source in a medium with a linear refractive index and a linear current profile. A linear convergence (with respect to the time step) of the numerical solution to the analytical one has been confirmed. Demonstration calculations have been performed of long-range sound propagation in an irregular ocean waveguide where detection of multiple arrivals represents an important part of the problem. In all cases the new algorithm revealed good performance in terms of stability and accuracy.

Moving fluids are acoustically anisotropic. Successful generalization of the HWT algorithm to acoustic fields in moving media indicates that the algorithm can be further extended to describe propagation of seismic waves in anisotropic solids.

We expect that, within the geometrical acoustics approximation, the new wavefront tracing software would allow one to efficiently model effects of "spice", internal gravity waves, and other physical processes in the water column on temporal structure of the acoustic field and on the spatial structure of wavefronts and time fronts in the ocean. Acoustic travel-time bias, multi-pathing, rapid proliferation of eigenrays, deep acoustic shadow-zone arrivals, and other previously studied effects[17–19,29,35–40] caused by random internal gravity waves and mesoscale inhomogeneities in the ocean can be modeled using this tool without neglecting currents. The HWT algorithm ability to accurately account for wind and its large- and small-scale variations is crucial for modeling long-range propagation of infrasound in the atmosphere.[41,42] Computational efficiency of the wavefront-tracing algorithm makes the approach suitable for large-scale Monte-Carlo simulations and for extensions to modeling sound propagation in three-dimensional inhomogeneous moving media.

Acknowledgments

This research was supported by the Office of Naval Research grant no. N00014-11-1-0048.

References

1. J. D. Benamou, An introduction to Eulerian geometrical optics (1992–2002), *J. Sci. Comput.* **19** (2003) 63–93.
2. J. A. Sethian, *Level Set Methods and Fast Marching Methods Evolving Interfaces in Computational Geometry, Fluid Mechanics, Computer Vision, and Materials Science* (University Press, Cambridge, 1999).
3. B. Engquist, E. Fatemi and S. Osher, Numerical resolution of the high frequency asymptotic expansion of the scalar wave equation, *J. Comp. Phys.* **120** (1995) 145–155.
4. S. Fomel and J. A. Sethian, Fast-phase space computation of multiple arrivals, *Proc. Natl. Acad. Sci.* **99** (2002) 7329–7334.
5. J. Qian and S. Leung, A level set based Eulerian method for paraxial multivalued traveltimes, *J. Comp. Phys.* **197** (2004) 711–736.
6. P. Sava and S. Fomel, 3-D traveltime computation using Huygens wavefront tracing, *Geophysics* **66** (2001) 883–889.
7. J. E. Vidale, Finite-difference calculation of traveltimes in three dimensions, *Geophysics* **55** (1990) 521–526.

8. V. Vinje, K. Åstebøl, E. Iversen and H. Gjøystdal, 3-D ray modeling by wavefront construction in open models, *Geophysics* **64** (1999) 1912–1919.
9. V. Vinje, E. Iversen and H. Gjøystdal, Traveltime and amplitude estimation using wavefront construction, *Geophysics* **58** (1993) 1157–1166.
10. K. Chambers and J.-M. Kendall, A practical implementation of wave front construction for 3-D isotropic media, *Geophys. J. Int.* **174** (2008) 1030–1038.
11. S. Gray and W. May, Kirchhoff migration using eikonal equation travel-times, *Geophysics* **59** (1994) 810–817.
12. L. M. Brekhovskikh and O. A. Godin, *Acoustics of Layered Media. 2: Point Sources and Bounded Beams*, 2nd edn. (Springer, Berlin, 1999).
13. M. Koch, A numerical study on the determination of the 3-D structure of the lithosphere by linear and non-linear inversion of teleseismic travel times, *Geophys. J. R. Astron. Soc.* **80** (1985) 73–93.
14. M. S. Sambridge, Non-linear arrival time inversion: Constraining velocity anomalies by seeking smooth models in 3-D, *Geophys. J. Int.* **102** (1990) 653–677.
15. O. A. Godin, D. Yu. Mikhin and S. Ya. Molchanov, Inverse problem of ray acoustics of moving medium, *Izv. AN SSSR. Fiz. Atmos. Okeana* **27** (1991) 139–150.
16. M. Bruneton, V. Farra and H. A. Pedersen, Non-linear surface wave phase velocity inversion based on ray theory, *Geophys. J. Int.* **151** (2002) 583–596.
17. M. G. Brown, J. A. Colosi, S. Tomsovic, A. L. Virovlyansky, M. A. Wolfson and G. M. Zaslavsky, Ray dynamics in long-range deep ocean sound propagation, *J. Acoust. Soc. Am.* **113** (2003) 2533–2547.
18. J. Simmen, S. M. Flatté and G.-Y. Wang, Wavefront folding, chaos, and diffraction for sound propagation through ocean internal waves, *J. Acoust. Soc. Am.* **102** (1997) 239–255.
19. L. J. Van Uffelen, P. F. Worcester, M. A. Dzieciuch, D. L. Rudnick and J. A. Colosi, Effects of upper ocean sound-speed structure on deep acoustic shadow-zone arrivals at 500- and 1000-km range, *J. Acoust. Soc. Am.* **127** (2010) 2169–2181.
20. J. L. Spiesberger, Comparison of measured and modeled temporal coherence of sound near 75 Hz and 3683 km in the Pacific Ocean, *J. Acoust. Soc. Am.* **124** (2008) 2805–2811.
21. F. Mulargia and S. Castellaro, Nondiffuse elastic and anelastic passive imaging, *J. Acoust. Soc. Am.* **127** (2010) 1391–1396.
22. O. A. Godin, Cross-correlation function of acoustic fields generated by random high-frequency sources, *J. Acoust. Soc. Am.* **128** (2010) 600–610.
23. O. A. Godin, N. A. Zabotin and V. V. Goncharov, Ocean tomography with acoustic daylight, *Geophys. Res. Lett.* **37** (2010) L13605.
24. M. G. Brown, Noise interferometry in an inhomogeneous environment in the geometric limit, *J. Acoust. Soc. Am.* **130** (2011) EL173–EL179.
25. J. A. Sethian, Evolution, implementation, and application of level set and fast marching methods for advancing fronts, *J. Comput. Phys.* **169** (2001) 503–555.
26. J. van Trier and W. W. Symes, Upwind finite-difference calculation of travel-times, *Geophysics* **56** (1991) 812–821.
27. P. Sava and S. Fomel, Huygens wavefront tracing: A robust alternative to conventional ray tracing, SEP report 95 (1997), pp. 101–113.
28. O. A. Godin, Helmholtz-Kirchhoff integral theorem for waves in a flow of inhomogeneous compressible fluid, *Dokl. Akad. Nauk* **358**, 614–617. [English translation: *Doklady Phys.* **43**, 84–87 (1998).]
29. O. A. Godin, V. U. Zavorotny, A. G. Voronovich and V. V. Goncharov, Refraction of sound in a horizontally-inhomogeneous, time-dependent ocean, *IEEE J. Oceanic Eng.* **31** (2006) 384–401.

30. O. A. Godin, Stability of acoustic wave fronts propagating in anisotropic three-dimensional environments, *Acta Acust. United Ac.* **95** (2009) 963–974.
31. O. A. Godin and A. G. Voronovich, Fermat's principle for non-dispersive waves in nonstationary media, *Proc. R. Soc. Lond. A* **460** (2004) 1631–1647.
32. C. L. Pekeris, Theory of propagation of sound in a half-space of variable sound speed under conditions of formation of a shadow zone, *J. Acoust. Soc. Am.* **18** (1946) 295–315.
33. Y. L. Li, C. H. Liu and S. J. Franke, Three dimensional Green's function for a wave propagation in a linearly inhomogeneous medium — The exact analytic solution, *J. Acoust. Soc. Am.* **87** (1990) 2285–2291.
34. W. Munk, P. Worcester and C. Wunsch, *Ocean Acoustic Tomography* (Cambridge University Press, Cambridge, 1995).
35. D. Makarov, S. Prants, A. Virovlyansky and G. Zaslavsky, *Ray and Wave Chaos in Ocean Acoustics*: *Chaos in Waveguides* (World Scientific, Singapore, 2010).
36. A. L. Virovlyansky, *Ray Theory of Long-Range Sound Propagation in the Ocean* (Inst. Applied Phys., Nizhny Novgorod, 2006) [in Russian].
37. O. A. Godin, Restless rays, steady wavefronts, *J. Acoust. Soc. Am.* **122** (2007) 3353–3363.
38. F. D. Tappert and X. Tang, Ray chaos and eigenrays, *J. Acoust. Soc. Am.* **99** (1996) 185–195.
39. O. A. Godin, A 2-D description of sound propagation in a horizontally-inhomogeneous ocean, *J. Comput. Acoust.* **10** (2002) 123–151.
40. A. L. Virovlyansky, A. Yu. Kazarova and L. Ya. Lyubavin, Ray-based description of shadow zone arrivals, *J. Acoust. Soc. Am.* **129** (2011) 2851–2862.
41. D. P. Drob, M. Garces, M. Hedlin and N. Brachet, The temporal morphology of infrasound propagation, *Pure Appl. Geophys.* **167** (2010) 437–453.
42. R. S. Matoza, J. Vergoz, A. Le Pichon, L. Ceranna, D. N. Green, L. G. Evers, M. Ripepe, P. Campus, L. Liszka, T. Kvaerna, E. Kjartansson and A. Hoskuldsson, Long-range acoustic observations of the Eyjafjallajokull eruption, Iceland, April-May 2010, *Geophys. Res. Lett.* **38** (2011) L06308.